Title

Nonlinear bounce resonances between magnetosonic waves and equatorially mirroring electrons

Journal

Journal of Geophysical Research Space Physics, 120(8)

ISSN

2169-9380

Authors

Chen, Lunjin
Maldonado, Armando
Bortnik, Jacob
et al.

Publication Date

2015-08-01

DOI

10.1002/2015ja021174

Peer reviewed

AGU PUBLICATIONS

JGR

Journal of Geophysical Research: Space Physics

RESEARCH ARTICLE

10.1002/2015JA021174

Key Points:
- Bounce resonance oscillation is nonlinear
- Bounce resonance enables subsequent scattering due to gyroresonance
- Bounce resonance is effective for first few harmonics of bounce frequency

Correspondence to:
L. Chen,
lunjin.chen@gmail.com

Citation:
Chen, L., A. Maldonado, J. Bortnik, R. M. Thorne, J. Li, L. Dai, and X. Zhan (2015), Nonlinear bounce resonances between magnetosonic waves and equatorially mirroring electrons, *J. Geophys. Res. Space Physics*, *120*, 6514–6527, doi:10.1002/2015JA021174.

Received 2 MAR 2015
Accepted 2 JUN 2015
Accepted article online 5 JUN 2015
Published online 26 AUG 2015

Nonlinear bounce resonances between magnetosonic waves and equatorially mirroring electrons

Lunjin Chen[1], Armando Maldonado[1], Jacob Bortnik[2], Richard M. Thorne[3], Jinxing Li[3], Lei Dai[4], and Xiaoya Zhan[5]

[1]Department of Physics, University of Texas at Dallas, Richardson, Texas, USA, [2]Department of Atmospheric and Oceanic Sciences, University of California, Los Angeles, California, USA, [3]Institute of Space Physics and Applied Technology, Peking University, Beijing, China, [4]State Key Laboratory of Space Weather, Center for Space Science and Applied Research, Chinese Academy of Sciences, Beijing, China, [5]Shenzhen Institute of Advanced Technology, Chinese Academy of Sciences, Shenzhen, China

Abstract Equatorially mirroring energetic electrons pose an interesting scientific problem, since they generally cannot resonate with any known plasma waves and hence cannot be scattered down to lower pitch angles. Observationally it is well known that the flux of these equatorial particles does not simply continue to build up indefinitely, and so a mechanism must necessarily exist that transports these particles from an equatorial pitch angle of 90° down to lower values. However, this mechanism has not been uniquely identified yet. Here we investigate the mechanism of bounce resonance with equatorial noise (or fast magnetosonic waves). A test particle simulation is used to examine the effects of monochromatic magnetosonic waves on the equatorially mirroring energetic electrons, with a special interest in characterizing the effectiveness of bounce resonances. Our analysis shows that bounce resonances can occur at the first three harmonics of the bounce frequency ($n\omega_b$, $n = 1$, 2, and 3) and can effectively reduce the equatorial pitch angle to values where resonant scattering by whistler mode waves becomes possible. We demonstrate that the nature of bounce resonance is nonlinear, and we propose a nonlinear oscillation model for characterizing bounce resonances using two key parameters, effective wave amplitude $\tilde{A}$ and normalized wave number $\tilde{k}_z$. The threshold for higher harmonic resonance is more strict, favoring higher $\tilde{A}$ and $\tilde{k}_z$, and the change in equatorial pitch angle is strongly controlled by $\tilde{k}_z$. We also investigate the dependence of bounce resonance effects on various physical parameters, including wave amplitude, frequency, wave normal angle and initial phase, plasma density, and electron energy. It is found that the effect of bounce resonance is sensitive to the wave normal angle. We suggest that the bounce resonant interaction might lead to an observed pitch angle distribution with a minimum at 90°.

1. Introduction

Energetic electrons in the radiation belts undergo three periodic motions: gyration, bounce, and drift. The three periodic motions have well-separated periods and each of them can be associated with an adiabatic invariant, referred to as the first, second, and third invariants [*Schulz and Lanzerotti*, 1974]. The presence of plasma waves can violate the invariants through wave-particle resonant interactions, leading to irreversible changes in electron phase space density [*Thorne*, 2010]. The process of wave-particle interaction plays an important role in the variability of the radiation belt electrons. Much more attention has been paid to gyroresonance and drift resonance interaction than bounce resonance, which can be responsible for the violation of the second invariant. Violation of the third invariant through drift interaction with ULF waves [e.g., *Dai et al.*, 2013] can lead to radial diffusion while violation of the first invariant through gyroresonance interaction can lead to pitch angle and energy scattering. It was suggested about five decades ago [*Parker*, 1961; *Roberts and Schulz*, 1968] that electrons can be subject to scattering by means of bounce resonance with hydrodynamic waves, when the wave frequency is equal to multiples of the bounce frequency. Recently, the idea of bounce resonance was brought up again [*Shprits*, 2009] to provide a potential mechanism for the observed global coherent variability of the radiation belt electron flux [*Kanekal et al.*, 2001; *Shprits et al.*, 2007]. Specifically, during geomagnetic storms, the radiation belt electron fluxes may vanish rapidly at all L shells, indicating that electrons at all equatorial pitch angles are effectively scattered by waves. This is also true for equatorially mirroring electrons with equatorial pitch angles $\alpha_{eq} = 90°$. However, those electrons are generally immune to the

gyroresonance interaction, which requires a finite electron velocity component along the field line to satisfy the gyroresonance condition unless the relativistic mass correction is sufficient to reduce the electron gyrofrequency to match the wave frequency. However, when the relativistic correction factor is relatively small, it appears the electrons with $\alpha_{eq} = 90^{\circ}$ cannot be resonantly scattered by the waves.

Equatorial noise [*Russell et al.*, 1969], also known as fast magnetosonic waves or ion Bernstein mode waves [*Gary et al.*, 2010], are electromagnetic emissions confined within a few degrees of the equator [e.g., *Santolík et al.*, 2004; *Hrbáčková et al.*, 2015], occurring above the proton gyrofrequency f_{cp} and below the lower hybrid resonance frequency f_{LHR}. The dominant component of the wave's magnetic field component is along the background magnetic field, with average amplitudes of ~50 pT [*Ma et al.*, 2013]. Much more intense magnetosonic waves have also been reported with amplitudes up to ~1 nT [*Tsurutani et al.*, 2014]. These waves can be excited with nearly perpendicular wave normal angles (and hence near-perpendicular propagation) at multiples of the ion gyrofrequency, by ring velocity distributions of ring current energetic protons [e.g., *Perraut et al.*, 1982; *Meredith et al.*, 2008; *Chen et al.*, 2010, 2011]. It has been shown that these waves undergo Landau resonance interaction responsible for electron acceleration [*Horne et al.*, 2007] and additional transit time scattering [*Bortnik and Thorne*, 2010; *Li et al.*, 2014]. Their frequencies typically range from a few hertz to 100 Hz, and the low-frequency portion of the wave band is close to the bounce frequency of energetic electrons above hundreds of keV [*Shprits*, 2009]. In this paper, we investigate the characteristics of bounce resonances of equatorially mirroring energetic electrons with equatorial noise. We will address this problem using a test particle approach, described in section 2, and present simulation results in section 3. In section 4, a nonlinear oscillation model is proposed to explain the nature of bounce resonance. The dependence of bounce resonance on various parameters is examined in section 5, followed by conclusions and a discussion in section 6.

2. Test Particle Model

The effects of electron bounce resonance due to magnetohydrodynamics (MHD) waves was previously investigated using the guiding center approach [*Roberts and Schulz*, 1968]. This is appropriate since the Larmor radius of electrons of interest is very small compared with the wavelength of MHD waves. For the fast magnetosonic waves above the proton gyro frequency f_{cp}, the wavelength can be comparable or even less than Larmor radius of relativistic electrons investigated in this study. For this reason, we adopt a set of relativistic test particle equations following *Bortnik and Thorne* [2010], where the particle motion is averaged over gyrophase but the finite Larmor radius effect remains. Taking advantage of the fact that equatorially mirroring electrons of interest are far from the conditions of gyroresonance and harmonic gyroresonances, the adopted equations for the electron bounce motion in the presence of a monochromatic magnetosonic wave can be reduced to

$$\frac{dp_z}{dt} = -\frac{p_\perp^2}{2m_e B_0 \gamma}\frac{\partial B_0(z)}{\partial z} + \sin\phi\left(J_1(\beta)\frac{eB_x^w p_\perp}{\gamma m_e} - J_0(\beta)eE_z^w\right)g(\lambda) \tag{1}$$

$$\frac{dp_\perp}{dt} = \frac{p_\perp p_z}{2m_e B_0 \gamma}\frac{\partial B_0(z)}{\partial z} - \sin\phi J_1(\beta)(eB_x^w v_z + eE_y^w)g(\lambda) \tag{2}$$

$$\frac{d\phi}{dt} = \omega - k_z v_z \tag{3}$$

$$\frac{dz}{dt} = v_z, \tag{4}$$

where t is time, z is the distance along the field line measured from the equator with the Northern (Southern) Hemisphere taken as positive (negative), p_z and $p_\perp$ are components of the electron's momentum parallel and perpendicular to the background magnetic field, v_z is the parallel component of electron velocity, e is the elementary charge, m_e is the electron rest mass, and γ is the electron Lorentz factor. The first terms of equations (1) and (2) on the right hand sides represent the adiabatic effect of the background dipole magnetic field, where $B_0(z) = B_{dip}h(\lambda)/L^3$ is the magnetic field strength along a dipole field line having an L shell of L, $B_{dip} = 0.31 \times 10^{-4}$ T is the surface magnetic field at the Earth's equator, and

$h(\lambda) = \sqrt{1+3\sin^2\lambda}/\cos^6\lambda$ representing latitudinal variation. For the dipole magnetic field, latitude λ is related to z through $\mathrm{d}z/\mathrm{d}\lambda = LR_E\cos\lambda\sqrt{1+3\sin^2\lambda}$ (the Earth radius $R_E = 6.37\times10^6$ m). The effect of the monochromatic wave (of angular frequency ω) is represented by the second terms of equations (1) and (2) on the right hand sides, where E_i^w and B_i^w are ith component of wave electric and magnetic field at the equator, respectively, and $g(\lambda)$ denotes the latitudinal variation of the wave amplitude. Without loss of generality, we assume wave vector **k** is contained in the x-z plane so that **k**'s perpendicular component $k_\perp = k_x > 0$ and $k_z > 0$, and also assume the wave amplitude for the parallel component of wave magnetic field B_z^w is positive so the x component amplitude of wave magnetic field $B_x^w = -k_\perp/k_z B_z^w$. The components of **k** and the amplitude of the wave electric field components E_x^w, E_y^w, and E_z^w can be determined by the cold plasma dispersion relation for magnetosonic waves. $\beta = \frac{k_\perp p_\perp}{eB_0}$ is the argument of Bessel functions J_0 and J_1, representing the ratio of the Larmor radius to the wavelength of the magnetosonic wave and therefore the effect of finite Larmor radius. ϕ in equations (1)–(3) represents the wave phase along the field line (or experienced by the center of the electron's gyromotion). It should be noted that although equatorially mirroring electrons are out of gyroresonances with the magnetosonic wave, Landau resonance is still possible when perturbed, i.e., where v_z becomes finite and matches ω/k_z (equation (3)). Since we are interested in the equatorially mirroring electrons, the initial conditions are set to be $z|_{t=0} = 0$, $p_z|_{t=0} = 0$, and $\phi|_{t=0} = \phi_0$ (denoting initial wave phase at the equator) and $p_\perp|_{t=0}$ is determined by electron kinetic energy (KE).

To set up the nearly perpendicularly propagating magnetosonic wave fields, we specify a wave normal angle θ near 90°and a wave frequency above the proton gyrofrequency ω_{cp} and below the lower hybrid resonance frequency ω_{LHR}. Given ω, θ, and wave magnetic amplitude B^w, the cold plasma dispersion relation in a magnetized electron and ion plasma for magnetosonic waves, which are the low-frequency extension of right-handed polarization whistler mode waves, is used to obtain the wave vector **k** and wave amplitude of electric and magnetic field components. For nearly perpendicular propagation, wave magnetic field fluctuation (B_z^w) is dominant in the parallel component and therefore possesses linear polarization. Since magnetosonic waves are fairly confined near the equator, we adopt a Gaussian latitudinal distribution of wave amplitude,

$$g(\lambda) = \exp(-\lambda^2/(\delta\lambda^w)^2) \tag{5}$$

with half width $\delta\lambda^w = 3°$ centered at $\lambda = 0°$. The calculation of the dispersion relation requires a plasma density distribution (N_e), which is reasonably assumed to be constant along the field line because of wave equatorial confinement.

For the case of electrons moving in the purely dipolar magnetic field, i.e., there is no wave field (the second right-hand side terms of equations (1) and (2) vanish), the electron's motion in z is analogous to the 1-D motion in a potential well with effective potential $\Phi_{\mathrm{eff}}(z) = \mu B_0(z)/\gamma^2$, where the magnetic moment μ is an adiabatic invariant and γ is conserved. Figure 1a shows an example of such potential along the magnetic field line of $L = 6.6$ and μ value corresponding to electrons of kinetic energy KE = 300 keV with the equatorial pitch angle $\alpha_{\mathrm{eq}} = 90°$. The minimum value of Φ_{eff} at $z = 0$ results in a periodic bounce motion about the equator along the field line. This is also true for equatorially trapped electrons with $\alpha_{\mathrm{eq}} = 90°$ (i.e., locating at the potential minimum) when subject to infinitesimal perturbation, and the motion along z is a harmonic oscillation with bounce frequency ω_b given by

$$\omega_b^2 = \frac{\mu}{\gamma^2 m_e}\left.\frac{\mathrm{d}^2B_0(z)}{\mathrm{d}z^2}\right|_{z=0} = \frac{\mu}{\gamma^2 m_e}\frac{9B_0(z=0)}{(LR_E)^2}. \tag{6}$$

Figures 1b and 1c show harmonic oscillations of latitude λ and local pitch angle α, respectively, for an electron with energy KE = 300 keV and equatorial pitch angle $\alpha_{\mathrm{eq}} = 89.9°$over the first five bounce periods ($T_b = 2\pi/\omega_b = 0.53$ s, corresponding to a bounce frequency of $\omega_b = 11.3$ rad/s). In the regime of small perturbation ($|z/(LR_E)| << 1$) of equatorially mirroring electrons, the amplitude of the latitude change $\Delta\lambda$ and the amplitude in pitch angle change $\Delta\alpha$ are related simply through $|\Delta\lambda/\Delta\alpha| = \sqrt{2}/3$.

3. Simulation Results

For the test particle simulation, equations (1)–(4) are solved numerically. For the nominal case, we launch electrons at the equator at $L = 6.6$ with an initial equatorial pitch angle $\alpha_{\mathrm{eq}} = 90°$and KE = 300 keV

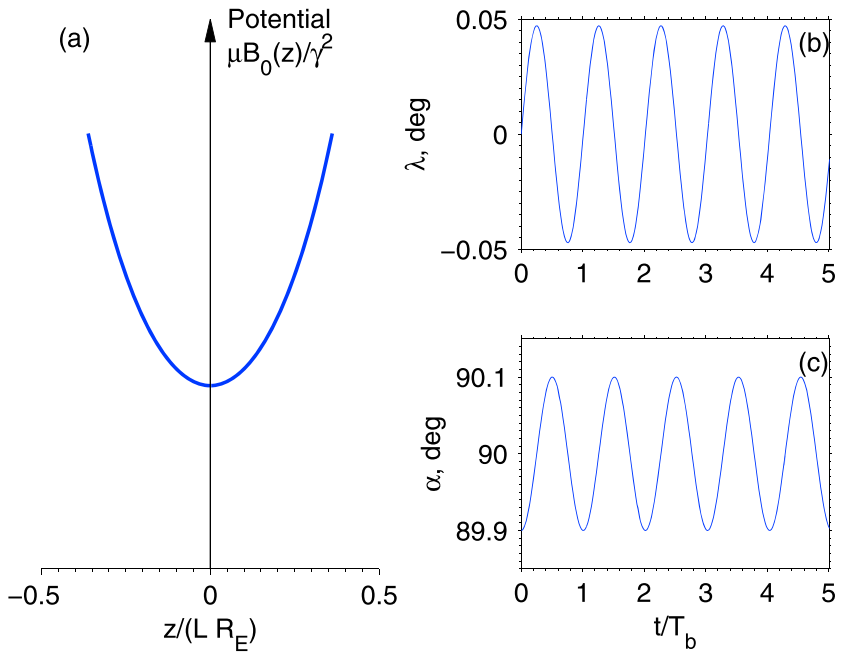

Figure 1. (a) Effective potential Φ_{eff} associated with electron motion along the field line as a function of z normalized by LR_E. (b) Latitude λ and (c) local pitch angle α for the bounce motion of electron with kinetic energy 300 keV and equatorial pitch angle 89.9°, as a function of time t normalized by the bounce period T_b.

(with a corresponding bounce period $T_b = 0.53$ s and bounce frequency $\omega_b = 11.3$ rad/s), in a wave field with $B^w = 50$ pT, $\theta = 88°$, $\phi_0 = 180°$ and varying wave frequency ω. The equatorial proton gyrofrequency at $L = 6.6$, $\omega_{cp} = 10.1$ rad/s, slightly below the electron bounce frequency ω_b. We vary the magnetosonic wave frequency ω in the range from just above ω_{cp} to 6.5 ω_b. Each test particle run is carried out over 200 T_b (~100 s). Figure 2 shows the response of the local pitch angle α for different wave frequencies (represented by different rows). Clearly, much larger amplitude oscillations in α (away from 90°) are obtained when the frequency ω matches $1\omega_b$ (Figure 2a), $2\omega_b$ (Figure 2c), and $3\omega_b$ (Figure 2e) than when ω is away from multiples of bounce frequency (Figures 2b, 2d, and 2f). The former cases illustrate the resonance between wave periodic forces and electron periodic bounce motions that occurs when the bounce resonance condition $\omega = n\omega_b$ is satisfied, where n is an integer. The value of the equatorial pitch angle α_{eq} can be seen by the lower envelope of the line plot of α. Principal bounce resonance with $\omega = \omega_b$ leads to α_{eq} change of ~10°and harmonic bounce resonances with $\omega = 2\omega_b$ and $\omega = 3\omega_b$ result in α_{eq} change of ~5°. Those bounce resonant responses also exhibit modulation in oscillation amplitudes. When out of bounce resonance for $\omega/\omega_b = 3/2$ (Figure 2b), 5/2 (Figure 2d), and 7/2 (Figure 2f), the change is only $<\sim 1°$. It is interesting to note that for this nominal case there is no resonant response at $\omega = 4\omega_b$ (Figure 2g) and higher harmonic frequencies (not shown).

To understand the nature of the bounce resonance, the time interval 10–40 T_b of the third harmonic resonance (Figure 2e) is selected for detailed examination. Figure 3 shows (a) local pitch angle α, (b) magnetic moment μ (blue line) and relativistic factor γ (green line), (c) Landau resonance parameter $\omega - k_z v_z$, (d) wave phase ϕ, and (e) the ratio of wave frequency to instantaneous bounce frequency ω/ω_b. When the Landau resonance parameter $\omega - k_z v_z$ approaches 0, Landau resonance occurs, where wave phase ϕ varies slowly (equation (3)), and results in a net change in the electron parallel momentum p_z (equation (1)). Over 10–20 T_b, α variation shows two frequency components at ω_b and ω (=$3\omega_b$); the amplitude at ω_b grows and the amplitude at $3\omega_b$ decays (Figure 3a). The variation becomes large and quasi-periodic with a single period T_b over 25–30 T_b, and then later decays to smaller amplitude. The development of bounce motion away from the equatorial plane has the following two consequences. First, the electron is able to mirror off the equator, and experience the fine spatial variation of wave amplitude along the field line. The spatial confinement of the magnetosonic waves results in a small net change (< 0.2%) of magnetic moment μ (Figure 3b). This effect is also known as transit time scattering [*Bortnik and Thorne*, 2010]), which can cause additional diffusion in energy and pitch angles. Second, the large amplitude of α variation away from 90°allows a finite v_z, which, when sufficient, enables the Landau resonance ($\omega - k_z v_z = 0$) as shown in Figure 3c. Occurrence of Landau resonance can

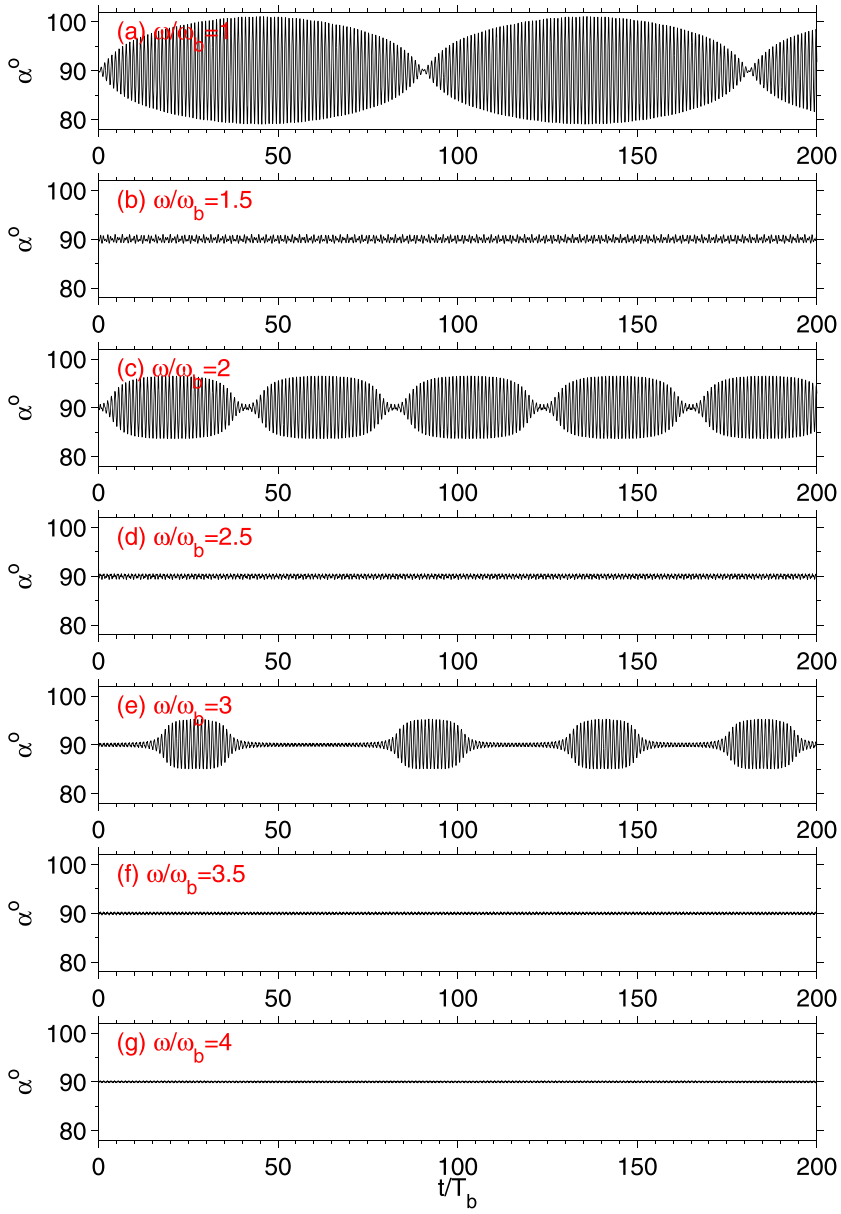

Figure 2. Local pitch angle as a function of time normalized by bounce period T_b, for electrons launched at the equator at $L = 6.6$ with initial pitch angle 90°and energy 300 keV, driven by a monotonic magnetosonic wave with varying wave frequency f = (a) 1.0 f_b, (b) 1.5 f_b, (c) 2.0 f_b, (d) 2.5 f_b, (e) 3.0 f_b, (f) 3.5 f_b, and (g) 4.0 f_b.

also be seen in the wave phase ϕ plot (Figure 3d). The change in ϕ reverses during Landau resonance (e.g., the highlighted red lines in Figure 3d near 23, 26, and 33 T_b,), while away from Landau resonance, ϕ complete three cycles (6π) within one bounce period (e.g., the highlighted red line near 13–16 T_b with 18π variation in ϕ over three bounce periods).

The effects of the magnetosonic waves on the electron include bounce resonance, transient scattering, and Landau resonance. Bounce resonance with equatorial mirroring electrons enables the latter two effects. Although Landau resonance also can produce a net change in p_z, the growth of p_z amplitude (and thus α amplitude and γ) is predominately due to the bounce resonance, because Landau resonance, if any, can only be effective over a small fraction of the bounce period. Landau resonance and transient scattering occur simultaneously when bounce oscillation is large, but it is transient scattering instead of Landau resonance that is mainly responsible for the small net change of μ in Figure 3b.

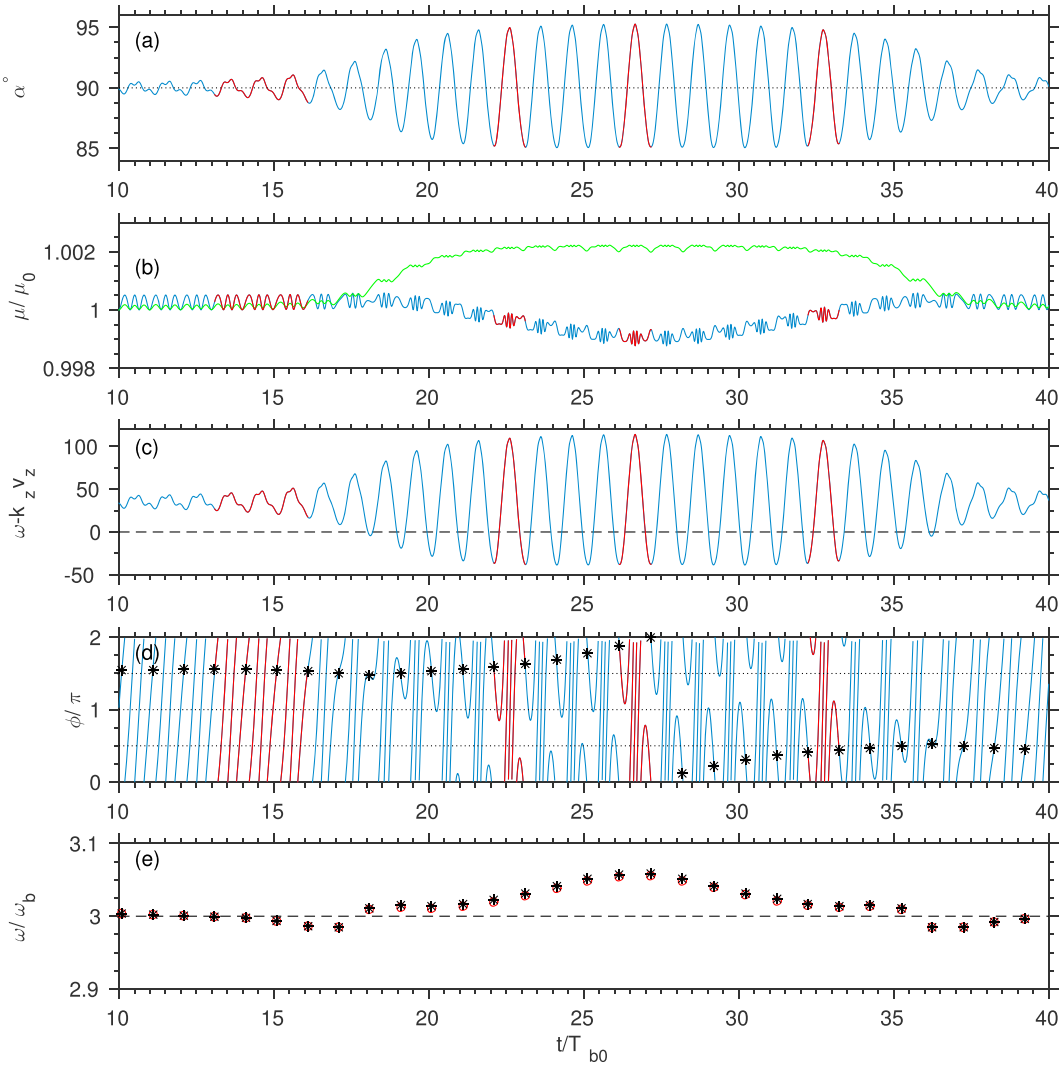

Figure 3. Detail analysis of the third harmonic bounce resonance example shown in Figure 2e. (a) Local pitch angle, (b) magnetic moment normalized by initial value μ/μ_0, (c) $\omega - k_z v_z$, (d) wave phase ϕ, and the ratio of wave frequency to electron bounce frequency. The horizontal dash line in Figure 3c denotes the line of Landau resonance. The black asterisks denote times when the electron crosses the equator from south to north. For viewing purpose, four segments of time intervals are highlighted as red lines.

It is important to note that the bounce frequency ω_b is not a constant value when large-amplitude bounce motion develops. The black asterisks of Figure 3e denote the ratio ω/ω_b. Instantaneous ω_b is evaluated numerically by calculating the time difference of every two successive equatorial crossings, when the electron is traveling toward the north. There exists a nonlinear tuning of ω_b so that ω/ω_b can slightly deviate from the initial value of 3. We will explain the source of this nonlinear tuning in the next section. This nonlinear turning of the bounce frequency is important for growth, decay and saturation of the bounce motion amplitude. The wave phases ϕ_{eq} at equatorial crossing from south to north are marked by black asterisk symbols in Figure 3d. ϕ_{eq} also represents phase difference at these equatorial crossing between wave phase and bounce phase ϕ_b of z in the bounce oscillation, where ϕ_b is defined as 0 at the equator moving toward to the north, $\pi/2$ at the north mirror point, and π at the equator moving toward the south, and $3\pi/2$ at the south mirror point. The oscillation amplitude grows when ϕ_{eq} near $3\pi/2$, saturates (neither grows nor decays) when ϕ_{eq} near 0 or 2π, and decays when ϕ_{eq} near $\pi/2$. When the oscillation amplitude is small ($10T_b < t < 20T_b$), there is no tuning of bounce frequency, so that ϕ_{eq} remains constant ($3\pi/2$) after each bounce motion (because ω/ω_b is an integer) and oscillation amplitude grows. When the oscillation amplitude is large ($20T_b < t < 30T_b$), nonlinear tuning leads to an increase of ω/ω_b (not an integer) so ϕ_{eq} increments after each bounce period and the

amplification due to bounce resonance reduces. Continuing tuning near $30T_b$ results in the shifting of ϕ_{eq} toward $\pi/2$, and oscillation amplitude decays until nonlinear tuning vanishes. This nonlinear tuning mechanism explains oscillation amplitude modulation shown in Figure 2.

4. Simplified Nonlinear Oscillation Model

Equations (1)–(4) described in the previous section contains various physical components: relativistic motion, adiabatic effect due to the background magnetic field, the finite Larmor radius effects, transient scattering associated with latitudinal distribution $g(\lambda)$, bounce resonance and Landau resonance (the $\omega - k_z v_z$ term). For understanding bounce resonance, a simplified nonlinear oscillation model in z is proposed here. We assume that magnetic moment μ and electron energy γ are conserved to the first order of p_z. The two assumptions are reasonable because both vary only by $<\sim 0.2\%$ (Figure 3b) and the relative change of γ due to the change of p_z is a second-order term for equatorially mirroring electrons. Therefore, the governing equation for the bounce motion reduce to

$$\frac{dp_z}{dt} = -\frac{\mu}{\gamma}\frac{\partial B_0(z)}{\partial z} + \sin(\omega t - k_z z + \phi_0)\left(-J_0(\beta)eE_z^w - \frac{2J_1(\beta)}{\beta}\frac{B_z^w k_z \mu}{\gamma}\right) g(\lambda) \tag{7}$$

The reduced equation is equivalent to equations (10) and (11) of *Roberts and Schulz* [1968] in the limit of $\beta = 0$ ($J_0(\beta) = 1$ and $\frac{2J_1(\beta)}{\beta} = 1$) when the finite Larmor radius effect disappears .

Rewriting in nondimensional quantities using $\tilde{z} = z/(LR_E)$, $\tilde{t} = \omega_b t$, $\tilde{k}_z = k_z LR_E$, and $\tilde{\omega} = \omega/\omega_b$ yields a nonlinear oscillation model of a second-order differential equation for $\tilde{z}$:

$$d^2\tilde{z}/d\tilde{t}^2 + \tilde{z} + \frac{39}{18}\tilde{z}^3 = -\tilde{A}\sin(\tilde{\omega}\tilde{t} - \tilde{k}_z\tilde{z} + \phi_0)g(\lambda) \tag{8}$$

$$\tilde{z}|_{\tilde{t}=0} = d\tilde{z}/d\tilde{t}|_{\tilde{t}=0} = 0 \tag{9}$$

where the linear term and the nonlinear cubic term on the left-hand side arise from the adiabatic change, the first two terms on the left-hand side are responsible for harmonic bounce oscillations, and the nonlinear sine term on the right-hand side is driven by the wave with initial wave phase at the equator ϕ_0 and normalized wave amplitude at the equator,

$$\tilde{A} = \frac{B_z^w k_z LR_E}{9B_0}\frac{2J_1(\beta)}{\beta} + \frac{E_z^w J_0(\beta) eLR_E\gamma}{9\mu B_0}. \tag{10}$$

The normalized $\tilde{A}$ contains the contribution from B_z^w and E_z^w and the effect of finite Larmor radius. For the parameters investigated in this paper, the term due to B_z^w is generally about 2 orders of magnitude greater than the term due to E_z^w, meaning that oscillating magnetic mirror force of the magnetosonic wave dominates over the wave parallel electric force.

When $|\tilde{k}_z\tilde{z}| \ll 1$, linearization of equation (8) yields

$$d^2\tilde{z}/d\tilde{t}^2 + \tilde{z}(1 - \tilde{A}\tilde{k}_z\cos(\tilde{\omega}\tilde{t} + \phi_0)) = -\tilde{A}\sin(\tilde{\omega}\tilde{t} + \phi_0) \tag{11}$$

where only linear terms of $\tilde{z}$ were kept. This linear equation is a driven Mathieu equation, which permits unstable solutions (i.e., bounce resonance solution) when $\tilde{\omega}$ is $2/q$, where q is an integer. When resonance occurs, the $\tilde{z}$ amplitude increases and then nonlinear terms cannot be ignored and the linear equation is not applicable. One consequence of nonlinear effect is fine tuning of bounce frequency, resulting in the change of relative phase between wave and bounce motion and the net effect of bounce resonance, because the change (growth, decay, and saturation) of oscillation amplitude depends on the phase difference (as illustrated in Figure 3). There are a few sources of nonlinear tuning, when $\tilde{z}$ amplitude is large. First, the change of magnetic moment μ and electron energy γ can lead to the change of ω_b (equation (6)). But the change of both appear to be small. Second, the cubic term might lead to an increase of ω_b by $O(\tilde{z}^2)$. Third, the nonlinear sine term can cause an increase or decrease of ω_b, depending on the wave phase at the equator ϕ_{eq}. The third term associated with the sine term is a major factor for tuning bounce frequency, which is to be proven below.

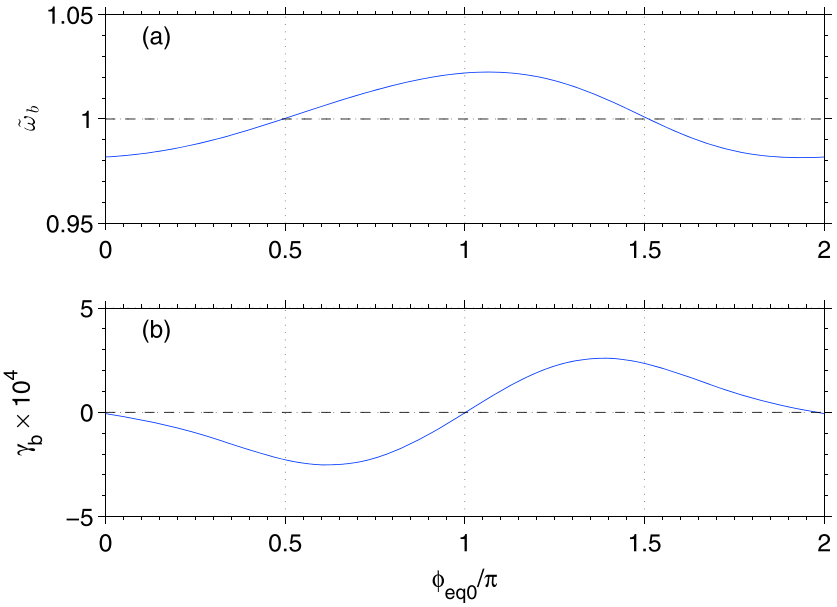

Figure 4. The dependence of (a) bounce frequency $\tilde{\omega}_b$ and (b) temporal change of the amplitude of $\tilde{z}$ oscillation on the initial equatorial wave phase ϕ_{eq0}.

Using the nominal parameter set in previous section, we obtain $\tilde{A} = 4.4 \times 10^{-3}$ and $\tilde{k}_z = 1.55 \times 10^2$. We solve for time period $\tilde{T}_b$ to complete a bounce using equation (8) without the cubic term,

$$d^2\tilde{z}/d\tilde{t}^2 + \tilde{z} = -\tilde{A}\sin(\tilde{\omega}\tilde{t} - \tilde{k}_z\tilde{z} + \phi_{eq0})g(\lambda) \tag{12}$$

where ϕ_{eq0} represents the initial wave phase at the equator and is assumed to be variable. Initial conditions are set to be $\tilde{z}|_{\tilde{t}=0} = 0$ and $d\tilde{z}/d\tilde{t}|_{\tilde{t}=0} = 0.04$, where the value of 0.04 corresponds to the oscillation amplitude over 25–30 T_b in Figure 2. Figure 4 shows the calculated bounce frequency $\tilde{\omega}_b (= 2\pi/\tilde{T}_b)$ and temporal change of oscillation amplitude γ_b as a function of ϕ_{eq0}. γ_b is defined as $\Delta\tilde{z}_{peak}/\tilde{T}_b$, where $\Delta\tilde{z}_{peak}$ is the difference of the two $\tilde{z}$ peaks over two successive bounce periods. For ϕ_{eq0} near π, $\tilde{\omega}_b > 1$ so that ϕ_{eq} increases when returning to the equator after one bounce period, and $\gamma_b \sim 0$ meaning that oscillation amplitude does not change. For ϕ_{eq0} near $\pi/2$, $\tilde{\omega}_b \sim 1$, and $\gamma_b > 0$, corresponding to the case of steady growth in amplitude, while for ϕ_{eq0} near $3\pi/2$, $\tilde{\omega}_b \sim 1$, and $\gamma_b < 0$, corresponding to the case of steady decay in amplitude. By using this nonlinear oscillation model (equation (12)), the obtained instantaneous ω_b are shown by red circles in Figure 3e, which matches well with ω_b obtained previously (black asterisks), that is, nonlinear tuning of bounce frequency is reproduced using the nonlinear sine term. We conclude that nonlinear tuning is mainly caused by the wave term, and amplitude modulation shown in Figure 3 is explained by the ϕ_{eq0} dependence of bounce frequency and of amplitude growth rate γ_b.

5. Frequency Response and Dependence on Wave and Particle Parameters

To measure the response of the equatorially mirroring electrons to the magnetosonic wave, we introduce the following three quantities: (1) the largest change in the equatorial pitch angle $|\Delta\alpha_{eq}|_{max}$, defined by the difference between the initial α_{eq} (=90°) and the minimum α_{eq}, $|\Delta\alpha_{eq}|_{max} = 90° - \min(\alpha_{eq})$; (2) the largest latitude reached, λ_{max}; and (3) the largest change in electron energy, $|\Delta\gamma|_{max} = \max(\gamma) - \gamma_0$. Note that γ_0 is the initial γ when $\alpha_{eq} = 90°$ and $\lambda = 0°$ and is also the minimum value of γ. In other words, any perturbation of α_{eq} will yield an increase in $|p_z|$ and thus an increase in electron kinetic energy, because μ and thus $p_\perp$ at the equator are quasi-invariant.

Using these definitions, we examine the dependence of the electron response on the initial wave phase ϕ_0. We use the same parameters as the nominal case except now we not only vary wave frequency ω with spacing of $0.1\omega_b$ and but also vary ϕ_0 from 0°to 360°with spacing of 15°(total 24 values of ϕ_0). Figure 5a shows the response of $|\Delta\alpha_{eq}|_{max}$ as a function of ω and ϕ_0. It is clearly shown that there are effective bounce resonances up to the third harmonic and no resonance is found beyond $3\omega_b$. While the bounce resonances at ω_b and $2\omega_b$

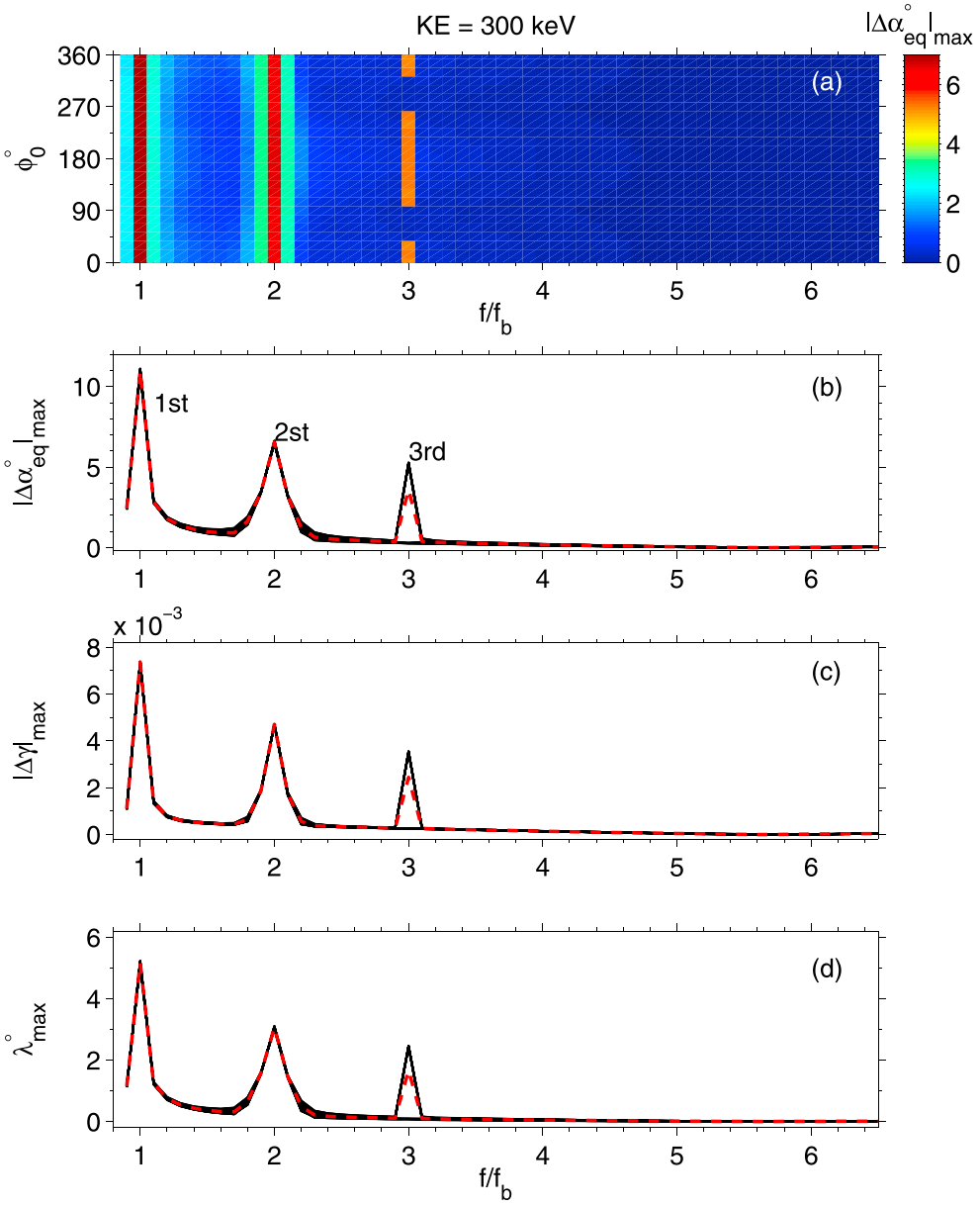

Figure 5. (a) Electron equatorial pitch angle change $|\Delta\alpha_{eq}|_{max}$ as a function of wave frequency f normalized by the electron bounce frequency f_b and initial wave phase ϕ_0. (b) the frequency response of $|\Delta\alpha_{eq}|_{max}$ for 24 different values of ϕ_0 (black lines) and its average over ϕ_0 (red line). (c and d) Similar to Figure 5b except for the frequency responses of $|\Delta\gamma|_{max}$ and λ_{max} respectively.

show little dependence of ϕ_0, the responses at third harmonic bounce resonance depend on ϕ_0, where little $|\Delta\alpha_{eq}|_{max}$ is produced near $\phi_0 \sim \pi/2$ or $3\pi/2$. One may interpret the sensitivity to the change of ϕ_0 as being an indication of a chaotic system. Slight changes in ϕ_0 while keeping the same initial conditions ($z|_{t=0} = 0$ and $p_z|_{t=0} = 0$) are equivalent to slight changes in the initial conditions while keeping ϕ_0 constant, with proper time-shifting. Any significant change of $|\Delta\alpha_{eq}|_{max}$ due to slight change of ϕ_0 (e.g., the third harmonic) means that the responses are dramatically different when the initial condition is perturbed, indicating the chaotic nature of the nonlinear system.

For the chosen wave parameters, the wave phase speed along the field line direction $v_{phz} = \omega/k_z = 2.4 \times 10^5$ m/s, and thus electrons initially with $KE = 300$ keV and $\alpha_{eq} = 90°$will require at least $|\Delta\alpha_{eq}|_{max}$ of 2.4°in order to satisfy the Landau resonance condition, $\omega - v_z k_z = 0$. This condition can be realized by the nonlinear oscillation driven by the same magnetosonic waves at frequencies near $\sim n\omega_b$ (n = 1,2, and 3) that are in

bounce resonance with electrons. Similarly, the change in α_{eq} is also sufficient for resonance with higher-frequency chorus waves, which requires a few degree deviation of α_{eq} from 90° [*Shprits*, 2009].

Figure 5b shows line plots of the frequency responses of $|\Delta\alpha_{eq}|_{max}$ for 24 different values of ϕ_0 (the black lines) and the frequency responses of $|\Delta\alpha_{eq}|_{max}$ averaged over ϕ_0 (the red dashed line). The effect of bounce resonance is also seen in the frequency responses of $|\Delta\gamma|_{max}$ and λ_{max}, shown in Figures 5c and 5d, respectively. As $|\Delta\alpha_{eq}|_{max}$ increases, so do $|\Delta\gamma|_{max}$ (corresponding to KE change of $|\Delta\gamma|_{max} \times 511$ keV) and λ_{max}. As mentioned above, the developed large-amplitude oscillation is a quasi-harmonic oscillation at ω_b, and thus, the relation among $|\Delta\gamma|_{max}$, λ_{max}, and $|\Delta\alpha_{eq}|_{max}$ can be established: $\lambda_{max} = \frac{\sqrt{2}}{3}|\Delta\alpha_{eq}|_{max}$ and $|\Delta\gamma|_{max} = \frac{\gamma_0^2-1}{2\gamma_0}|\Delta\alpha_{eq}|^2_{max}$ under the assumption of μ conservation. The former is linearly proportional to $|\Delta\alpha_{eq}|_{max}$, while the latter is proportional to $|\Delta\alpha_{eq}|^2_{max}$, indicating the relative change of electron energy is 1 order of magnitude less than the change of α_{eq} for those equatorially mirroring electrons in bounce resonance. These relations can be readily verified by the black lines of Figures 5c and 5d. For example, for the bounce resonance at ω_b, $|\Delta\alpha_{eq}|_{max} = 11°$ (from Figure 5b), and therefore, based on analytical relations above, $\lambda_{max} = 5.2°$and $|\Delta\gamma|_{max} = 0.0176$. The analytic λ_{max} value is identical to corresponding numerical result shown in Figure 5d while the analytical $|\Delta\gamma|_{max}$ is about twice the corresponding numerical $|\Delta\gamma|_{max}$ value (= 0.0073 in Figure 5c), which is due to small but finite change of μ mainly associated with transit time scattering.

To investigate the dependence of the electrons' responses on the wave and particle parameters, we will compare the frequency responses of the average $|\Delta\alpha_{eq}|_{max}$ over the initial wave phase (as shown by the red dashed line in Figure 5b). $|\Delta\alpha_{eq}|_{max}$ is used because responses of energy change $|\Delta\gamma|_{max}$ and responses of latitude change λ_{max} are related to $|\Delta\alpha_{eq}|_{max}$. The average of $|\Delta\alpha_{eq}|_{max}$ is done over the initial wave phase ϕ_0, because ϕ_0 is a random parameter independent of electrons and because $|\Delta\alpha_{eq}|_{max}$ might depend on ϕ_0. The response of the average $|\Delta\alpha_{eq}|_{max}$ shown by the red line in Figure 5b is selected as nominal case with electron initial kinetic energy KE = 300 keV, plasma density $N_e = 50$ cm^{-3}, wave normal angle $\theta = 88°$, wave peak amplitude $B^w = 50$ pT and $L = 6.6$. Compared with the nominal parameters, we calculate the frequency response of the average $|\Delta\alpha_{eq}|_{max}$ by increasing and decreasing one of the five parameters at a time while keeping the remaining four the same as the nominal case. In total, 11 sets of the five parameters are considered. Figure 6 shows the dependence of the frequency response of the average $|\Delta\alpha_{eq}|_{max}$ on these five parameters (KE, N_e, θ, B^w, and L shell), with the nominal response shown by black dashed lines in each panel. There are a few common features among the cases.

1. Bounce resonance occurs preferentially at the first three harmonics, and no resonance occurs above 4 ω_b.
2. Bounce resonance occurs over a narrow range of ω near $n\omega_b$ (n = 1, 2, 3), i.e., not necessarily at exact $n\omega_b$.
3. Bounce resonance at ω_b occurs for all the cases except for the case of KE = 0.1 MeV (the red line of Figure 6a) and the case of $L = 5$ (the blue line of Figure 6e). Both exceptions have smaller ω_b, which is below ω_{cp}, and therefore, resonance at $\omega = \omega_b$ is not considered because of the constraint of $\omega > \omega_{cp}$.
4. Bounce resonance at the second and third harmonics does not always occur. Examples include the case of KE = 1 MeV in Figure 6a, the case of $N_e = 10$ cm^{-3} in Figure 6b, and the case of $B^w = 20$ pT in Figure 6c, and the case of $L = 5$ in Figure 6e.
5. The response tends to be weaker for high harmonics and diminishes at fourth harmonic and above.

The dependence of the bounce resonance effect on these parameters can be understood through the nonlinear oscillation model introduced in equations (8) and (9) in section 4. Clearly, the solution of oscillation in $\tilde{z}$ is determined by two key parameters $\tilde{A}$ and $\tilde{k}_z$. For examining how the effect of principal bounce resonance depends on $\tilde{A}$ and $\tilde{k}_z$, we set $\tilde{\omega} = 1$ and $\phi_0 = \pi$ and solve equations (8) and (9) to obtain the maximum $\tilde{z}_{max}$ over $\tilde{t} < 400\pi$ at different combinations of $\tilde{A}$ and $\tilde{k}_z$. $\tilde{A}$ varies from 10^{-4} to 10^{-2} and $\tilde{k}_z$ ranges from 1 to 10^3, to be representative of magnetospheric conditions. $\tilde{z}_{max}$ can be readily translated to $|\Delta\alpha_{eq}|_{max}$ through the relation in the bounce motion. The result of $|\Delta\alpha_{eq}|_{max}$ as a function of $\tilde{A}$ and $\tilde{k}_z$ is shown in Figure 7a. Similarly, $|\Delta\alpha_{eq}|_{max}$ for $\tilde{\omega} = 2$, 3, and 4 are obtained and shown in Figures 7b–7d, respectively. For the principal bounce resonance $\tilde{\omega} = 1$, large $|\Delta\alpha_{eq}|_{max}$ (> 2°) occur in most of $\tilde{A}$ and $\tilde{k}_z$ regime. For harmonic bounce resonance $\tilde{\omega} = 2$, 3, and 4, there is a sharp boundary in $\tilde{A}$ and $\tilde{k}_z$ separating weak and strong response. The condition for strong response at higher harmonic resonance are more strict (favoring higher $\tilde{A}$ and $\tilde{k}_z$). The threshold for resonances at $\tilde{\omega} = 2$, 3, and 4 can be roughly approximated by the black dash lines, $\tilde{A}\tilde{k}_z^{0.82} = 9.04 \times 10^{-3}$, $\tilde{A}\tilde{k}_z^{0.88} = 0.13$, and $\tilde{A}\tilde{k}_z = 3.5$ in Figures 7b–7d, respectively.

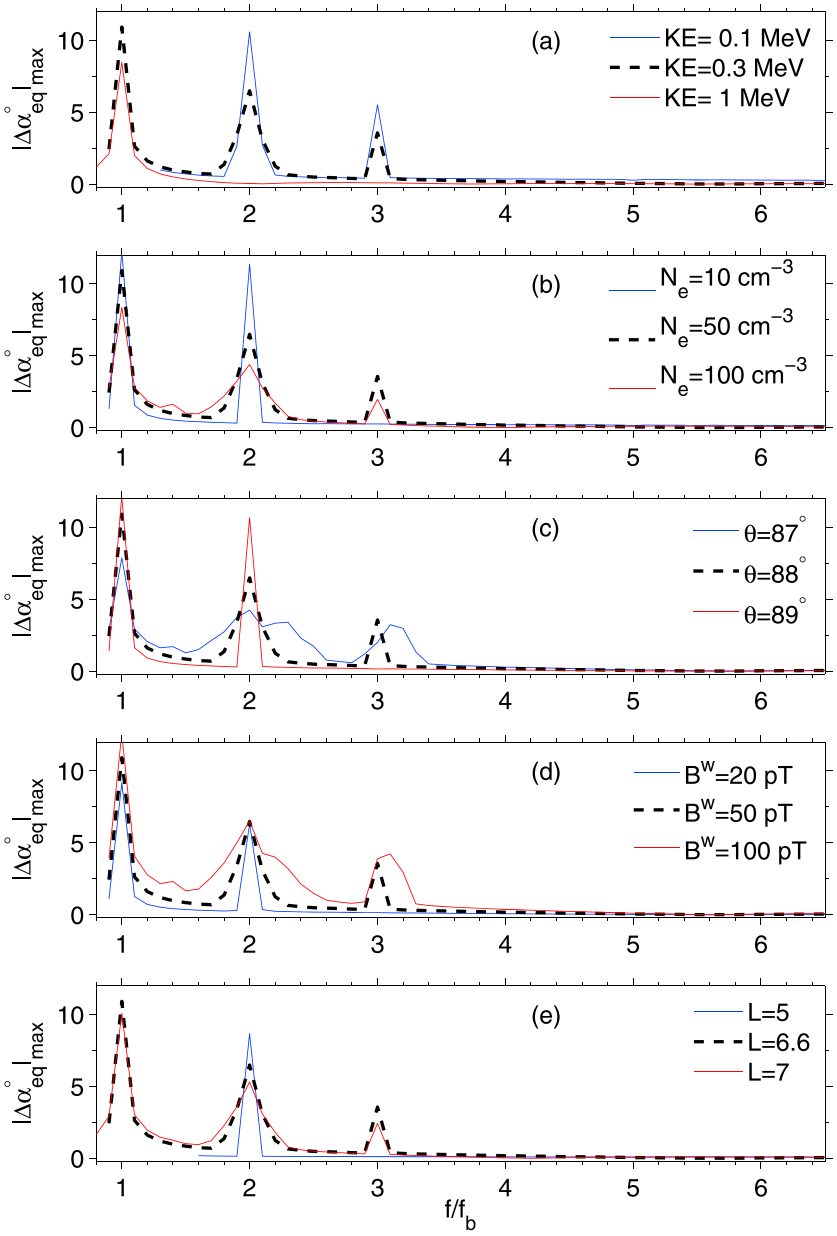

Figure 6. Dependence of the frequency response of the average $|\Delta\alpha_{eq}|_{max}$ on (a) electron kinetic energy KE, (b) plasma density N_e, (c) wave normal angle θ, (d) wave amplitude B^w at the equator, and (e) L shell value. The nominal case is shown by the black dashed lines with KE = 300 keV, $N_e = 50$ cm^{-3}, $\theta = 88°$, $B^w(\lambda = 0) = 50$ pT, and $L = 6.6$.

It is also worthwhile noting that $|\Delta\alpha_{eq}|_{max}$ of resonant response tends to have little dependence of wave amplitude and that although the threshold for effective resonances favors higher $\tilde{k}_z$, $|\Delta\alpha_{eq}|_{max}$ tends to decrease for higher $\tilde{k}_z$.

To compare with results from equations (1) and (2) for the 11 cases above, we calculate corresponding $\tilde{A}$ and $\tilde{k}_z$ and mark the cases having $|\Delta\alpha_{eq}|_{max} \geq 2°$with $\phi_0 = \pi$ and $\omega/\omega_b = 1$ in the $\tilde{A} - \tilde{k}_z$ map in Figure 7a as black pluses and the other cases as open circles. Similar procedures are done with $\omega/\omega_b = 2$ in Figure 7b, with $\omega/\omega_b = 3$ in Figure 7c, and with $\omega/\omega_b = 4$ in Figure 7d, respectively. Clearly, the nonlinear oscillation model predicts the effectiveness of resonant response at different harmonic frequencies, and the dependence on KE, N_e, θ, B^w, and L shell can be narrowed down to the dependence on the two key parameters $\tilde{A}$ and $\tilde{k}_z$. Increasing kinetic energy tends to have larger Larmor radius (and thus β) and effectively reduce $\tilde{A}$, which explains diminishing response at $2\omega_b$ and $3\omega_b$ for the case of KE = 1 MeV (the red line of Figure 6a).

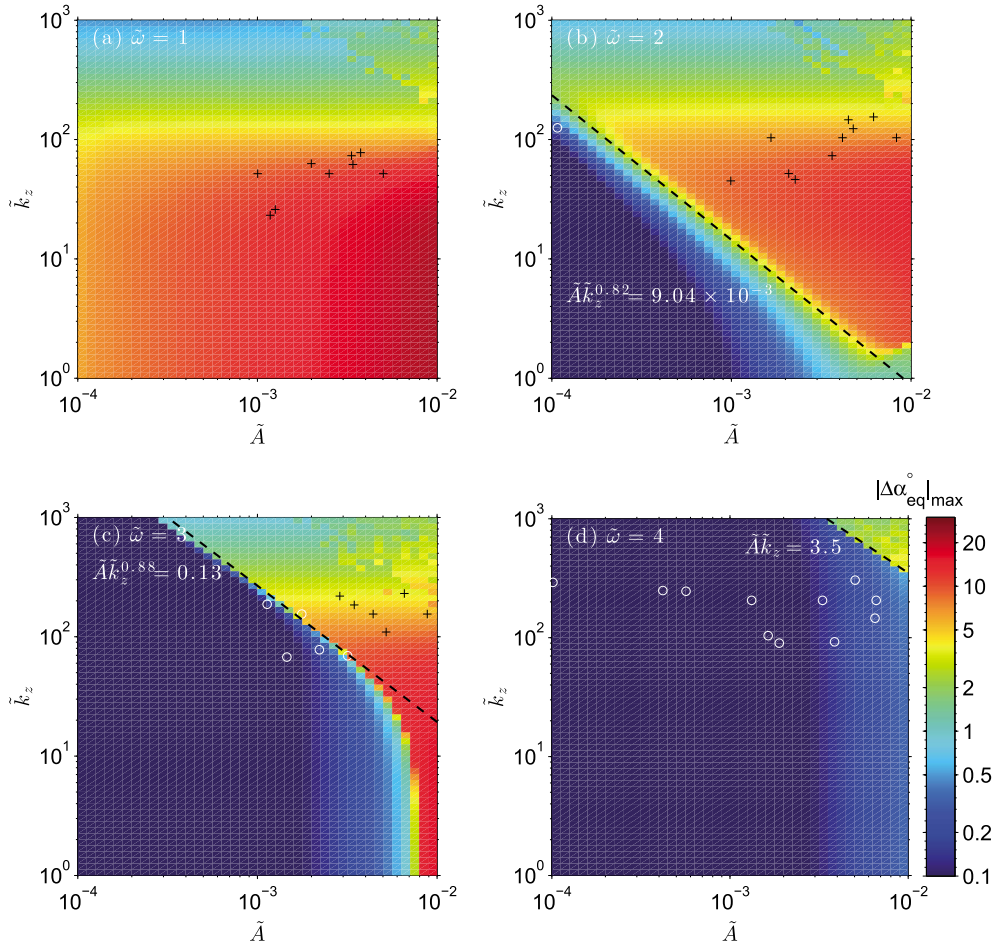

Figure 7. The response of $|\Delta\alpha_{eq}|_{max}$ for $\tilde{\omega}$ = (a) 1, (b) 2, (c) 3, and (d) 4, as a function of $\tilde{A}$ and $\tilde{k}_z$ of Equation (8). The black dashed lines in Figures 7b–7d, representing $\tilde{A}\tilde{k}_z^{0.82} = 9.04 \times 10^{-3}$, $\tilde{A}\tilde{k}_z^{0.88} = 0.13$, and $\tilde{A}\tilde{k}_z = 3.5$, approximate the boundary of $|\Delta\alpha_{eq}|_{max} = 2°$ in the response for $\tilde{\omega} = 2$, 3, and 4, respectively. Black pulses denote the cases among the 11 cases in Figure 6 having $|\Delta\alpha_{eq}|_{max} \geq 2°$, while white circles denote those cases having $|\Delta\alpha_{eq}|_{max} < 2°$.

Increasing N_e tends to increase $k_\perp$ and k_z, and thus increase $\tilde{A}$ and $\tilde{k}_z$. This accounts for diminishing responses at $3\omega_b$ for the case having the lowest $N_e = 10$ cm^{-3} (the blue line of Figure 6b). Increasing wave normal angle θ results in the decrease of $\tilde{k}_z$ and therefore the disappearance of resonances at $3\omega_b$ for the case of $\theta = 89°$ (the red line of Figure 6c). Since $\tilde{k}_z$ is sensitive to θ, a change of 1° in θ can lead to significantly different frequency response. This suggests that an accurate information for wave normal angle is needed for quantifying the effect of bounce resonance. Increasing wave amplitude B^w leads to the increase of $\tilde{A}$. The case of the lowest amplitude $B^w = 20$ pT is not sufficient for producing effective resonance at $3\omega_b$ (the blue line in Figure 6d). Finally, decreasing L leads to the increase of background magnetic field B_0 and thus the reduction of $\tilde{A}$. This explains no response at $3\omega_b$ for the case of $L = 5$ (the blue line in Figure 6e). For all the 11 cases considered, none of them lie in the regime (above the black dashed line of $\tilde{A}\tilde{k}_z = 3.5$ in Figure 7d) where resonance at $4\omega_b$ becomes effective.

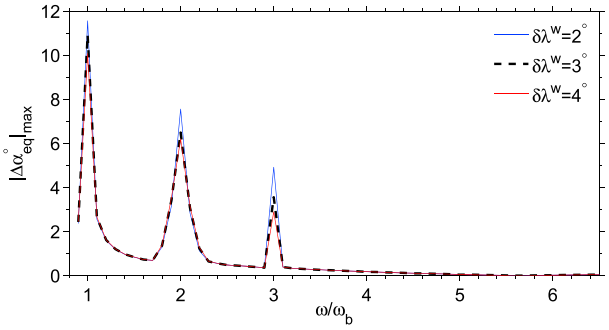

Figure 8. Dependence of $|\Delta\alpha_{eq}|_{max}$ response on the half latitudinal width of wave amplitude $\delta\lambda^w$.

We also check the dependence on the half latitudinal width $\delta\lambda^w$ of the wave amplitude. Figure 8 shows $|\Delta\gamma|_{max}$ as a function of wave frequency using the nominal set

of parameters for $\delta\lambda^w = 2°$, 3°, and 4°. The responses are almost identical except for a slight difference at $\omega = 3\omega_b$. All the three cases produce effective bounce resonance for the first three harmonics and no resonant effect at higher harmonics. So we conclude that although $|\Delta\gamma|_{\max}$ might vary slightly with $\delta\lambda^w$, it is combined $\tilde{A}$ and $\tilde{k}_z$, instead of $\delta\lambda^w$, that is crucial when determining whether a harmonic bounce resonance is effective.

6. Conclusions and Discussion

We have investigated the characteristics and dynamics of the interactions of equatorially mirroring energetic electrons with monochromatic magnetosonic waves using a test particle simulation and demonstrated that large-amplitude oscillations in the equatorial pitch angle can be produced due to bounce resonances. We also explored the dependence of the bounce resonance effects on various parameters, including electron kinetic energy, plasma density, wave normal angle, frequency, amplitude and initial phase, and *L* shell. Our principal conclusions are summarized as follows:

1. Bounce resonances with magnetosonic waves introduce nonlinear oscillations of equatorially mirroring electrons, which can enable the removal of those electrons out of the equatorial plane and also enable Landau resonance with the same waves and other wave emissions.
2. A nonlinear oscillation model is proposed to characterize the effects of magnetosonic waves on the equatorially mirroring electrons, with two key parameters $\tilde{A}$ and $\tilde{k}_z$.
3. Bounce resonances occur when $\omega \sim n\omega_b$ and are effective for the first few harmonic frequencies. Threshold for higher harmonic resonances requires higher $\tilde{A}$ and $\tilde{k}_z$.
4. The bounce oscillation amplitude caused by bounce resonance is sensitive to wave normal angle and $\tilde{k}_z$ of magnetosonic waves.

Bounce resonant interactions with the magnetosonic waves can reduce α_{eq} by a few degrees for initially equatorially mirroring electrons. This can effectively kick those electrons out of the equatorial plane over a few bounce periods. As a result, these electrons can obtain a sufficient v_z, which enables Landau resonance with magnetosonic waves and likely resonance with chorus waves too [e.g., *Tao et al.*, 2012]. Bounce resonance produces an oscillation but cannot by itself remove these electrons directly into the loss cone. Subsequent Landau resonance can lead to pitch angle and energy scattering and thus eventually the loss.

Bounce resonance might also lead to a reduction of the electron phase space density at $\alpha_{eq} = 90°$, thus creating a minimum near 90° in the equatorial pitch angle distribution. *Zhao et al.* [2014] recently reported a peculiar pitch angle distribution of relativistic electrons (several hundreds of keV) from Van Allen Probes observation in the inner radiation belt and the slot region, showing minima at 90° near the magnetic equator. We speculate that this might be the consequence of bounce resonance with equatorial noise during inward transport, through which electrons encounter the equatorial noise that provides bounce resonances. We will examine carefully simultaneous wave and particle measurement from Van Allen Probes for evidence of such bounce resonant effect.

Another consequence is scattering associated with bounce resonance. When nonlinear oscillation depends on wave phases (e.g., Figure 5a), bounce scattering can occurs, leading to electron scattering over a finite range of equatorial pitch angles α_{eq} near 90°. The range of α_{eq} is limited by $|\Delta\alpha_{eq}|_{\max}$. As illustrated in Figure 5a, the sensitive dependence on wave initial phase during the third harmonic bounce resonance indicates the chaotic nature of the bounce resonances while little dependence on wave initial phase for the first two harmonic resonances indicates the regular motion of the bounce resonances. The criteria to separate the regular and chaotic motion is beyond the scope of the current study and will be explored in the future studies. We have simplified the wave forces by considering a monochromatic wave. These will be also improved in the future by implementing multiple wave model.

Acknowledgments

The work at UTD was supported by NSF's Geospace Environment Modeling grant AGS-1405041 and NASA grant NNX15AF55G. UCLA authors would like to gratefully acknowledge the support of NSF's GEM grant AGS-1103064 and NSF/DOE basic plasma physics grant DE-SC0010578 in performing this work. No observational data are used in this work.

M. Balikhin thanks two anonymous reviewers for their assistance in evaluating this paper.

References

Bortnik, J., and R. M. Thorne (2010), Transit time scattering of energetic electrons due to equatorially confined magnetosonic waves, *J. Geophys. Res.*, *115*, A07213, doi:10.1029/2010JA015283.

Chen, L., R. M. Thorne, V. K. Jordanova, and R. B. Horne (2010), Global simulation of magnetosonic waves instability in the storm time magnetosphere, *J. Geophys. Res.*, *115*, A11222, doi:10.1029/2010JA015707.

Chen, L., R. M. Thorne, V. K. Jordanova, M. F. Thomsen, and R. B. Horne (2011), Magnetosonic wave instability analysis for proton ring distributions observed by the LANL magnetospheric plasma analyzer, *J. Geophys. Res.*, *116*, A03223, doi:10.1029/2010JA016068.

Dai, L., et al. (2013), Excitation of poloidal standing Alfvén waves through drift resonance wave-particle interaction, *Geophys. Res. Lett.*, *40*, 4127–4132, doi:10.1002/grl.50800.

Gary, S. P., K. Liu, D. Winske, and R. E. Denton (2010), Ion Bernstein instability in the terrestrial magnetosphere: Linear dispersion theory, *J. Geophys. Res.*, *115*, A12209, doi:10.1029/2010JA015965.

Horne, R. B., R. M. Thorne, S. A. Glauert, N. P. Meredith, D. Pokhotelov, and O. Santolík (2007), Electron acceleration in the Van Allen radiation belts by fast magnetosonic waves, *Geophys. Res. Lett.*, *34*, L17107, doi:10.1029/2007GL030267.

Hrbáčková, Z., O. Santolík, F. Němec, E. Macúšová, and N. Cornilleau-Wehrlin (2015), Systematic analysis of occurrence of equatorial noise emissions using 10 years of data from the Cluster mission, *J. Geophys. Res.*, *120*, 1007–1021, doi:10.1002/2014JA020268.

Kanekal, S., D. Baker, and J. Blake (2001), Multisatellite measurements of relativistic electrons: Global coherence, *J. Geophys. Res.*, *106*(A12), 29,721–29,732.

Li, J., et al. (2014), Interactions between magnetosonic waves and radiation belt electrons: Comparisons of quasi-linear calculations with test particle simulations, *Geophys. Res. Lett.*, *41*, 4828–4834, doi:10.1002/2014GL060461.

Ma, Q., W. Li, R. M. Thorne, and V. Angelopoulos (2013), Global distribution of equatorial magnetosonic waves observed by THEMIS, *Geophys. Res. Lett.*, *40*, 1895–1901, doi:10.1002/grl.50434.

Meredith, N. P., R. B. Horne, and R. R. Anderson (2008), Survey of magnetosonic waves and proton ring distributions in the Earth's inner magnetosphere, *J. Geophys. Res.*, *113*, A06213, doi:10.1029/2007JA012975.

Parker, E. N. (1961), Effect of hydromagnetic waves in a dipole field on the longitudinal invariant, *J. Geophys. Res.*, *66*(3), 693–708, doi:10.1029/JZ066i003p00693.

Perraut, S., A. Roux, P. Robert, R. Gendrin, J. Sauvaud, J. Bosqued, G. Kremser, and A. Korth (1982), A systematic study of ULF waves above F/H plus/ from GEOS 1 and 2 measurements and their relationships with proton ring distributions, *J. Geophys. Res.*, *87*, 6219–6236, doi:10.1029/JA087iA08p06219.

Roberts, C. S., and M. Schulz (1968), Bounce resonant scattering of particles trapped in the Earth's magnetic field, *J. Geophys. Res.*, *73*(23), 7361–7376.

Russell, C. T., R. E. Holzer, and E. J. Smith (1969), Ogo 3 observations of elf noise in the magnetosphere: 1. Spatial extent and frequency of occurrence, *J. Geophys. Res.*, *74*(3), 755–777.

Santolík, O., F. Nemec, K. Gereová, E. Macúšová, Y. Conchy, and N. Cornilleau-Wehrlin (2004), Systematic analysis of equatorial noise below the lower hybrid frequency, *Ann. Geophys.*, *22*, 2587–2595, doi:10.5194/angeo-22-2587-2004.

Schulz, M., and L. J. Lanzerotti (1974), *Particle Diffusion in the Radiation Belts*, Phys. and Chem. in Space, Springer, Berlin.

Shprits, Y., D. Kondrashov, Y. Chen, R. Thorne, M. Ghil, R. Friedel, and G. Reeves (2007), Reanalysis of relativistic radiation belt electron fluxes using crres satellite data, a radial diffusion model, and a Kalman filter, *J. Geophys. Res.*, *112*, A12216, doi:10.1029/2007JA012579.

Shprits, Y. Y. (2009), Potential waves for pitch-angle scattering of near-equatorially mirroring energetic electrons due to the violation of the second adiabatic invariant, *Geophys. Res. Lett.*, *36*, L12106, doi:10.1029/2009GL038322.

Tao, X., J. Bortnik, J. M. Albert, and R. M. Thorne (2012), Comparison of bounce-averaged quasi-linear diffusion coefficients for parallel propagating whistler mode waves with test particle simulations, *J. Geophys. Res.*, *117*, A10205, doi:10.1029/2012JA017931.

Thorne, R. M. (2010), Radiation belt dynamics: The importance of wave-particle interactions, *Geophys. Res. Lett.*, *37*, L22107, doi:10.1029/2010GL044990.

Tsurutani, B. T., B. J. Falkowski, J. S. Pickett, O. P. Verkhoglyadova, O. Santolik, and G. S. Lakhina (2014), Extremely intense ELF magnetosonic waves: A survey of polar observations, *J. Geophys. Res.*, *119*, 964–977, doi:10.1002/2013JA019284.

Zhao, H., X. Li, J. Blake, J. Fennell, S. Claudepierre, D. Baker, A. Jaynes, D. Malaspina, and S. Kanekal (2014), Peculiar pitch angle distribution of relativistic electrons in the inner radiation belt and slot region, *Geophys. Res. Lett.*, *41*, 2250–2257, doi:10.1002/2014GL059725.